journal

J. Am. Ceram. Soc., 79 [11] 2865–77 (1996)

Synthesis of Oxynitride Powders via Fluidized-Bed Ammonolysis, Part I: Large, Porous, Silica Particles

Clint R. Bickmore* and Richard M. Laine*

Department of Materials Science and Engineering and Department of Chemistry, University of Michigan, Ann Arbor, Michigan 48109-2136

Reaction of silica (SiO_2) with triethanolamine (TEA, $N(CH_2CH_2OH)_3$) and ethylene glycol (EG) under conditions (~200°C) where byproduct water is removed resulted in the formation of the neutral silatrane glycolate complex, $N(CH_2CH_2O)_3SiOCH_2CH_2OH$ (or $TEASiOCH_2CH_2OH$) in essentially quantitative yield. Solutions of this neutral precursor in EG, when rapidly pyrolyzed and then oxidized at 500°C, formed porous ceramic powders with high specific surface areas (>500 m^2/g). These powders were nitrided via ammonolysis in a fluidized-bed reactor at temperatures of 700°–1000°C. The resulting nitrided powders were characterized by thermal and chemical analyses, diffuse reflectance infrared spectroscopy, gas sorption, and X-ray photoelectron spectroscopy. The apparent activation energy for the nitridation process was determined to be 54 kJ/mol. Following nitridation, the powders were amorphous and had nitrogen contents as high as 21 wt% with retained surface areas >300 m^2/g at 1000°C. Under the nitridation conditions used, the extent of nitrogen incorporation correlated linearly with increases in material density. This linearity suggested that the change in density occurred primarily because of changes in coordination that occurred as trivalent nitrogen replaced divalent oxygen in the glass structure and nominally because of viscous flow. The linear density increase also suggested that pore trapping did not occur under these processing conditions. This work serves as a model for ongoing studies on the nitridation of high-surface-area ceramic powders produced by the rapid pyrolysis of mixed-metal TEA alkoxides.

I. Introduction

OXYNITRIDE glasses offer potential as lightweight structural ceramics, in particular as oxynitride-glass fibers in composites. By comparison with their oxide counterparts, they have superior mechanical properties, which are derived from the additional crosslinking obtained when trivalent nitrogen replaces divalent oxygen in the glass network.[1–6] The higher degree of crosslinking provides increased stiffness with a nominal increase in density, thereby displaying a higher relative modulus (elastic modulus/density). For example, the relative modulus of "S" glass increases from 36 to 43 $GPa\cdot(g/cm^3)^{-1}$ by introducing 3 at.% nitrogen.[1,2] Adding nitrogen also increases the glass-transition temperature.[1] Consequently, the viscosity of the nitrided glass is higher at any given temperature, manifesting a barrier to crystallization, because of sluggish atomic rearrangements, as well as the noted beneficial increase in stiffness.

Oxynitride glasses do not occur naturally; they must be synthesized and then processed to a desirable form. Our goal is to produce high-strength, oxynitride-glass fibers for composite applications.[7] The presumption is made that the fibers will be drawn from a glass boule; however, this does not preclude producing fibers via precursor processing methods. Two approaches predominate in processing oxynitride glasses: melt processing[8–11] and gas/solid nitridation.[12–24]

Melt processing entails melting compacts of mixed ceramic powders (oxides and nitrides) at high temperatures (1500°–1800°C) in nitrogen environments (1–10 atm (0.1–1 MPa)).[11] Homogenization of the powder compacts during melting is a diffusional process; therefore, the time required at elevated temperature increases as the melt viscosity, initial particle size, and heterogeneity of the initial powders increases.[11,25–28] The viscosity of the melt can be lowered by increasing the processing temperature; however, at higher temperatures, the nitrides are prone to decompose, according to[1]

$$Si_3N_4 \rightarrow 3Si + 2N_2 \quad (1)$$

$$Si_2N_2O \rightarrow SiO(v) + Si + N_2 \quad (2)$$

Two detrimental effects may result: elemental-silicon inclusions and gas bubbles. These shortcomings may be avoided by using lower temperature routes to oxynitride glasses, such as gas/solid nitridation.

Gas/solid nitridation entails heating a ceramic precursor (metal, metal oxide, organometallic, etc.) to moderate temperatures (400°–1200°C) in a nitriding environment (flowing NH_3, N_2, N_2H_4). Nitriding with NH_3, a process called ammonolysis, begins with reactions at the surface and may be generalized by the following:[1]

$$2SiO_2 + 2NH_3 \rightarrow Si_2N_2O + 3H_2O(v) \quad (3)$$

$$2SiO + 2NH_3 \rightarrow Si_2N_2O + H_2O(v) + 2H_2 \quad (4)$$

$$3SiO_2 + 4NH_3 \rightarrow Si_3N_4 + 6H_2O(v) \quad (5)$$

The reaction of NH_3 with the precursor surface is dominant in nitrogen incorporation. A mechanism for nitrogen incorporation was proposed by Mulfinger[12] and modified by others,[13] as depicted in Fig. 1. The schematic shows a simplified infinite surface, where the lines denote an artificial barrier between the solid and the vapor. This mechanism begins with the adsorption of NH_3 onto Lewis acid sites on the surface, where it first reacts to produce metal amide and hydroxyl groups (Fig. 1(a)). The amide and hydroxyl groups react further to produce a bridging imide and concurrently release a water molecule (H_2O) (Fig. 1(b)). Further condensation of the imide with another metal hydroxyl gives the metal nitride and coincidentally releases an additional water molecule (Fig. 1(c)). The law of mass action for ammonolysis predicts that the forward direction for reactions (3)–(5) will occur at low partial pressures of water.[1,12–23] Thus, ammonolysis requires the continual removal of water, which implies a dynamic-flow regime.

Even though nitridation is a surface event, the bulk phase and surface morphology can greatly affect the rate and extent of

C. G. Pantano—contributing editor

Manuscript No. 192137. Received December 18, 1995; approved May 26, 1996.
Supported by Army Research Laboratories through Contract No. DOD-C-DAAL04-91-C-0068, and the Army Research Office, through ASSERT Grant No. DOD-G-DAAL03-92-G-0053.
*Member, American Ceramic Society.

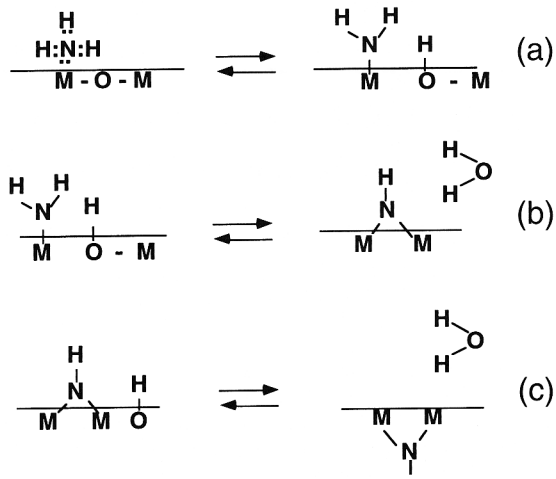

Fig. 1. NH_3 reacting with a metal oxide surface, producing a metal amide and an imide. ((a) reaction produces metal amide and hydroxyl groups; (b) further reaction produces a bridging imide and water is released; and (c) condensation with the imide with another metal hydroxyl produces a metal nitride and more water is released).

nitrogen incorporation. In the bulk phase, diffusion rates are generally much greater for amorphous materials than for their crystalline counterparts.[26] Consequently, amorphous precursors have the advantage of faster homogenization of nitrogen. The morphology of the ceramic precursor should be modified to obtain high specific surface areas (SSAs) to maximize reaction area and minimize diffusion distances. Continuous porosity within particles, such that the internal pores contribute significantly to the exposed surface area, provides a useful morphology. Therefore, highly porous, amorphous powders should serve as beneficial precursors to homogeneous oxynitride glasses.

Effective nitridation must balance the continual exchange of gaseous reactants and byproducts. During ammonolysis of SiO_2 (reaction (3)), water must be removed constantly to maintain favorable nitriding conditions. Fluidized-bed reactors (FBRs) are ideal for such reactions, because the fluidizing gas removes reaction byproducts while providing homogeneity in the bed. One drawback to fluidization is maintaining the force balance between the settling force on the particle and particle buoyancy resulting from the flowing gas. High buoyancy, common with ultrafine particles, results in entrainment rather than fluidization. For example, Wusirika,[17] in a systematic study on the ammonolysis of fumed silica (high surface area, amorphous powder) was able to obtain high-nitrogen-content SiO_xN_y glasses (<22 wt% nitrogen). Unfortunately, fumed silica is very fine and is entrained at the high flow rates required to sweep away byproduct water. One solution to this problem is to use coarser particles that contain extensive internal porosity. Coarse particles are also less prone to electrostatic agglomeration.[29] The nitrided coarse particles can then be comminuted to give more useful finer particles.

The goal of the work described here is to produce amorphous oxynitride powders by ammonolysis in an effort to evaluate and understand the parameters that lead to effective nitridation. The results of this work will be applied to the synthesis of multicomponent oxynitride glasses and fibers.[1,7,19] The approach we have taken is to develop a processing window for the pyrolytic conversion of the silatrane glycolate complex, $N(CH_2CH_2O)_3SiOCH_2CH_2OH$ (or $TEASiOCH_2CH_2OH$), to high-surface-area, amorphous oxide powders. These powders offer the desired high internal porosity, coupled with large particle sizes, and are, henceforth, called LPSPs (large, porous, silica particles; LPSPs refers to powders made by the two-step pyrolysis described in section II). The LPSPs are subsequently nitrided by heating in an ammonia FBR. The focus has been to define the processing window for nitridation based on the kinetic parameters, temperature, and time while monitoring surface area.

II. Experimental Procedure

(1) Synthesis

(A) Reagents: Amorphous silica (SiO_2) was received as a gift (Cab-O-Sil, Cabot, Tuscola, IL) and used as received (99.8% purity). Triethanolamine (TEA, $N(CH_2CH_2OH)_3$) was purchased (Aldrich Chemical, Milwaukee, WI) or received as a gift (Dow Chemical, Midland, MI). TEA from both sources was used as received (98%). Analytical- or reagent-grade ethylene glycol (EG, $HOCH_2CH_2OH$) was purchased (Mallinckrodt, Paris, KY). EG recovered from reactions (see below) was redistilled to remove water and recycled into the reactions.

(B) Silatrane Glycolate, $N(CH_2CH_2O)_3SiOCH_2CH_2OH$: Typical reaction conditions are as follows and are discussed in detail elsewhere. Silica (30 g, 0.5 mol) was mixed with 1 equiv TEA (75 g, 0.5 mol) in ~600 mL EG in standard schlenkware equipped with a mechanical stirrer and a still head. The mixture was heated under N_2, maintaining slow distillation (~200°C). Over a period of 8 h, ~1 L of EG and byproduct water were distilled off with periodic replenishment of EG. Concurrent with distillation, the solution became clear, where the clarity of the solution indicated complete reaction and formation of the silatrane glycolate complex. Once the solution cleared, distillation was continued to concentrate the solution until the still-head temperature exceeded the boiling point of EG (typically 205°–210°C). The solution was allowed to cool. The product yield is essentially quantitative.

(2) Powder Preparation

Pyrolysis and oxidation treatments were performed in a fused-silica process tube, as shown in Fig. 2. The process tube was assembled such that a tube (28 cm × 2.7 cm inside diameter) with one end closed was mounted to an O-ring ball joint, and the corresponding socket was fitted with a gas exit port and an Ace-Thred™ (Ace Glass, Vineland, NJ) tube fitting, which secures a gas inlet tube (7 mm inside diameter). The gas exit was fitted with a trap to condense evolved organics. Pyrolyses were conducted (Model Carbolite CTF 12/65, Bamford Mill, Sheffield, U.K.) in a vertical tube furnace equipped with a programmable controller and feedback thermocouple (Model 818P, Eurotherm, Reston, VA).

A two-step pyrolysis process, with the furnace held isothermally at 500°C, was used to convert the silatrane glycolate to an oxide powder. The first pyrolysis step was an isotherm for 4 h in flowing N_2 (250 mL/min) to decompose and evolve most of the organics from the sample. This step was begun by pouring the concentrated precursor solution (~50 g solution, 20 wt% ceramic yield) into the bottom of the process tube and then inserting the tube into the preheated furnace. (Note: care must be taken to trap the EG and volatile pyrolysis products that are produced during the pyrolysis.) After cooling, the powder was ground (−100 mesh) with an alumina mortar and pestle. The second pyrolysis step was a fixed-bed oxidation at 500°C for 24 h in flowing O_2 (500 mL/min) to oxidize residual carbon. The resulting material consisted of LPSPs.

(3) Nitridation

A FBR was used for ammonolysis, as shown in Fig. 3. The FBR was constructed with the following fused-silica components: a gas inlet tube (7 mm inside diameter), to feed NH_3 through the hot zone to the bottom of the furnace, and a process tube (25.4 mm diameter) fitted with a porous silica frit (coarse, 25.4 mm diameter; Ace Glass) as the diffuser. The control thermocouple is embedded in the furnace refractory; therefore, to compensate for the cooling effect of the gas flow, a calibration curve was created. The calibration curve was determined by attaching a chart recorder to a chromel–alumel thermocouple inserted into a fuzed-quartz closed tube with an outside diameter of 5 mm and positioned in the powder bed. The furnace was heated according to the standard heating schedules (see below), and sample temperatures were calculated from the chart. The furnace was located inside a fume hood during heat treatments.

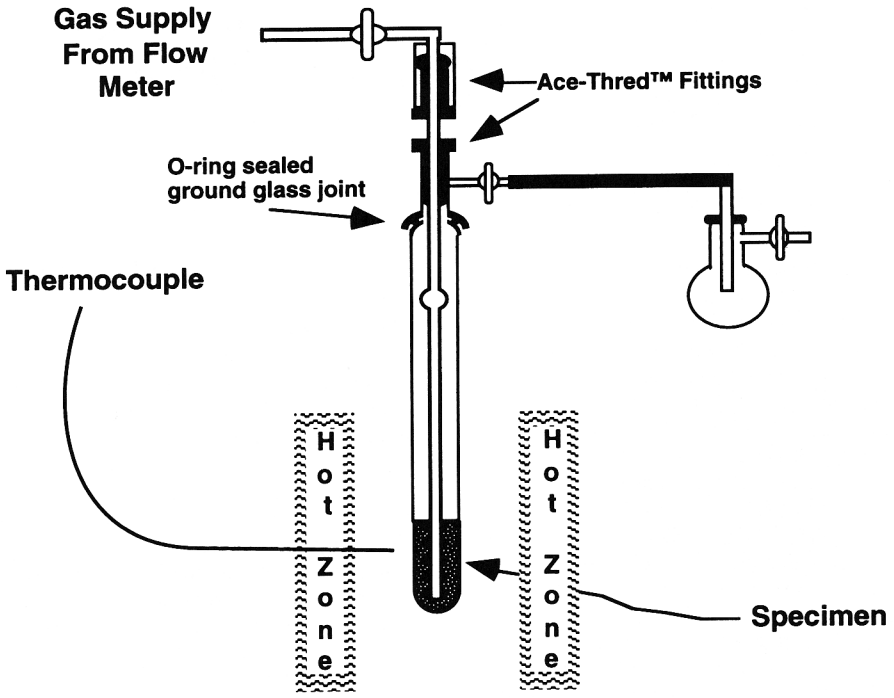

Fig. 2. Schematic of process tube fitted in tube furnace.

The ammonia supply was controlled by a solenoid, integrated with an automatic timer, and a safety shutoff, in case of a power failure.

Ammonolyses were conducted by loading amorphous oxide powder samples (1 g) onto the diffuser frit of the FBR, heating at 10°C/min to the desired furnace temperature (700°, 800°, 900°, or 1000°C), and holding isothermally for the desired time (4, 12, or 24 h) under flowing NH_3 (1.5 L/min). Temperatures are reported as furnace temperature, with the exception of the Arrhenius plot, which is plotted as sample temperatures (675°, 761°, 845°, and 938°C, determined from the calibration curve for the furnace temperatures shown above). The NH_3 flow rate of 1.5 L/min was set empirically by determining the state of full fluidization at ambient conditions.[30]

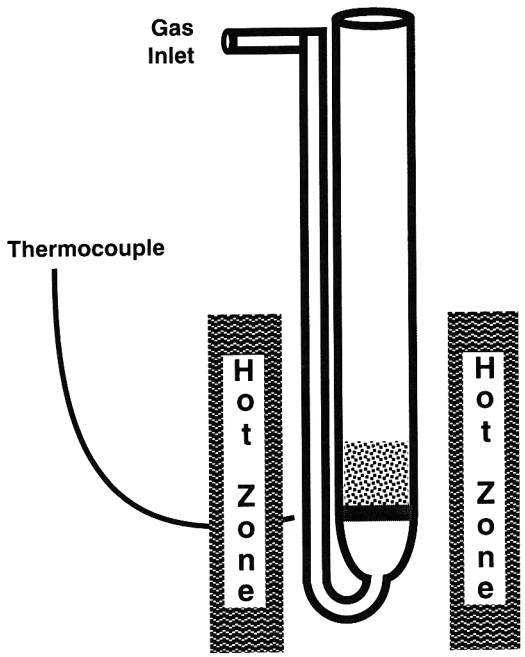

Fig. 3. Schematic of fluidized-bed reactor (FBR) fitted in tube furnace.

(4) Characterization

(A) Thermal Analysis: Thermogravimetric analysis (TGA) and differential thermal analysis (DTA) were performed (Thermal Analyst 2200 with Hi-Res™ TGA 2950, TA Instruments, New Castle, DE). TGA consisted of heating at constant ramp rates (10°, 20°, and 50°C/min) and dynamic HiRes TGA ramp rates of 50°C with a HiRes sensitivity of 4. The HiRes feature allows rapid heating rates that are dynamically modulated, thus they maintain high resolution during regions of weight loss by having a preset weight-loss rate trigger the dynamic ramp rate to slow. Dynamic ramp rates aid in separating closely stacked thermal events. The TGA balance flow meter was set at 40 mL/min N_2, whereas the purge flow meter was adjusted to 60 mL/min of either N_2 or dry air.

(B) Gas Sorption: Surface areas and pore-size distributions were determined by nitrogen adsorption at 77 K using the volumetric technique on a sorption analyzer (Model ASAP 2000M, Micromeritics Instrument Corp., Norcross, GA). Samples were degassed at 110°C for 2 h and then at 400°C until the outgas rate was <5 μm Hg/min (typically 4 h). The SSAs were determined by the Brünauer–Emmett–Teller (BET) multipoint method with at least five data points with relative pressures of 0.001–0.20. Pore-size distributions were determined with the density functional theory using the nitrogen on carbon at 77 K with the slitlike pores model. Analysis was performed using the software package supplied with the instrument.

(C) Scanning Electron Microscopy: Powder morphologies were examined by scanning electron microscopy (SEM) (Model S800, Hitachi, Tokyo, Japan) operated at 5 keV. The sample was affixed to the aluminum sample holder with an adhesive tab (Ted Pella, Redding, CA). The sample was sputter coated with gold/paladium for 45 s at 10 mV, which corresponds to a film thickness of 100 Å (10 nm).

(D) Diffuse-Reflectance Infrared Fourier Transform Spectroscopy: Diffuse-reflectance infrared Fourier transform (DRIFT) spectra[31–33] were obtained on a bench (Galaxy Series 3020, Mattson, Madison, WI) continuously purged with N_2, adapted with a diffuse reflectance accessory (Model DRA-2CO,

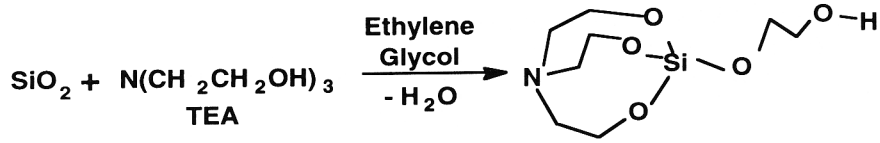

Fig. 4. Synthesis of the silatrane glycolate complex.

"Praying Mantis;" Harrick Scientific, Ossining, NY). The non-absorbing medium used was potassium bromide (KBr) (ICL, Garfield, NJ) powdered from a single crystal with an alumina mortar and pestle. Powder specimens were prepared as follows: (i) 0.3–0.5 wt% analyte was added to the KBr chunks (e.g., 2 mg analyte to 450 mg KBr); (ii) the mixture was ground with an alumina mortar and pestle; and (iii) the dilute samples were packed firmly in the sample holder, leveled off at the upper edge, and transferred to the FTIR sample chamber (brief exposure to air). Typical scan conditions were 1000 scans at 4 cm^{-1} resolution. All data are reported in Kubelka–Munk units, so that intensity values are nearly linear with concentration.

(E) Chemical Analysis: Samples were submitted for analysis of carbon, hydrogen, and nitrogen content (CHN);† CHN analysis (Model 2400 CHN Elemental Analyzer, Perkin-Elmer, Norwalk, CT) was performed at a temperature of 1075°C, with helium as a carrier gas. Powder specimens (1.5 mg) were loaded into tin capsules with powdered tin (6–10 mg) as a combustion aid. Acetanilide was used as a reference standard and was analyzed in the same manner as the samples. Each powder was analyzed twice. Both analyses were reported to give an indication of sample homogeneity.

(F) Helium Pycnometry: Density measurements for the samples were made using a helium pycnometer (Model AccuPyc 1330 V2.01, Micromeritics Instrument Corp.). Reported densities are an average of five values and have a standard deviation <0.003 g/cm^3.

(G) X-ray Photoelectron Spectroscopy: Chemical binding states were determined by X-ray photoelectron spectroscopy (XPS) (Model PHI 5400 XPS, Perkin-Elmer). The X-ray source was Mg*K* (1253.6 eV) operated at 15 kV and 300 W. The analysis chamber was maintained at 5×10^{-9} torr ($\sim 7 \times 10^{-7}$ Pa). The analyzer pass energy was 17.9 eV in steps of 0.1 eV. Powder specimens were pressed by hand between two sheets of indium foil; the sheets were separated, and one was mounted to the specimen holder. Tabulated values were taken as midpoints from full width at half maximum (FWHM) of the plotted data.

(H) X-ray Diffractometry: Samples were analyzed by powder X-ray diffractometry (XRD) with a rotating anode goniometer (Rigaku Denki Co. Ltd., Tokyo, Japan). Specimens (25 mg) were dusted on a glass specimen holder swabbed with petroleum jelly and placed in the diffractometer. Scans were measured from 5°–80° 2θ at a scan speed of 1° 2θ/min in 0.05° 2θ increments with monochromatic Cu$K\alpha$ (λ = 0.154 nm) radiation operated at 40 kV and 100 A. Peak positions were referenced to standard International Centre for Diffraction Data (ICDD, Newtowne Square, PA) files.

†CHN analysis was performed by the Department of Chemistry analytical services, University of Michigan.

III. Results

(1) Synthesis

The silatrane glycolate complex is synthesized by reaction of mixtures of silica powder with TEA in EG (Fig. 4). Reaction occurs best when the mixture is heated to EG distillation temperatures. TEA is a triol that reacts to form a tridentate "silatrane" complex.[34] The reaction goes to completion such that only the product remains in the reaction vessel. The reaction byproduct is water, which is removed along with distilling EG. On complete reaction, the solution is concentrated such that pourability is maintained at room temperature.

On heating, the silatrane complex will undergo condensation and ring-opening polymerization to form oligomers and polymers.[34] Initiation of the polymerization process is suggested by dimerization, as shown in Fig. 5. As will become evident, such polymerization reactions appear to be necessary to develop the highly porous microstructure that results during pyrolysis.

(2) Powder Preparation

Pyrolysis is the chemical decomposition or other chemical change brought by the action of heat. TGA decomposition studies of the precursor solution used to prepare LPSPs give insight into how thermal processing may affect the resulting powder properties. Three modes of mass loss are exhibited in Fig. 6: volatilization, decomposition, and oxidation. The first mass loss (ambient to <350°C) results primarily from volatilization of EG from excess solvent and as a byproduct of condensation (Fig. 5). The amount of excess EG present and the extent of polymerization (in solution) greatly affect the precursor viscoelastic properties and the ceramic yield. The loss of EG has the direct effect of increasing the viscosity.

The remaining two modes of mass loss correspond to the conversion of the precursor to a ceramic. The second mode of loss (325°–375°C) is due to decomposition of the organic ligands. The mass loss triggers the dynamic ramp rate to slow the heating rate to a nearly stepwise isothermal condition (~345°C). During decomposition, the organic portion of the precursor is destroyed, marking the transition to a ceramic. The third mode of loss (375°–700°C) is due to oxidation of residual organic matter and pyrolytic carbon (~10 wt%). Oxidation commences with decomposition (second mode) and extends to temperatures >700°C; however, because oxidation exhibits more dependence on time than temperature, isothermal treatments can be substituted. Figure 6 shows a ceramic yield of 20 wt%, as compared to the theoretical yields of 25.5% and 29.3% for the products in Figs. 4 and 5. The decomposition temperature delineates the lower boundary for bulk pyrolysis.

Pyrolysis conducted on the precursor above the decomposition temperature results in the formation of a ceramic as well as organic byproducts. The byproducts are important in the development of the powder morphology, as will be discussed.

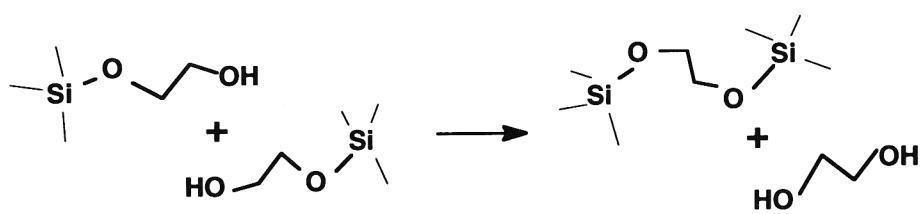

Fig. 5. Condensation dimerization of silatrane glycolate complex.

The precursor solution can be rapidly pyrolyzed to leave a porous ceramic, which, after oxidation of pyrolytic carbon, exhibits a pore-size distribution as shown in Fig. 7 (see two-step pyrolysis in section II(*2*)). The pore-size distribution appears to be trimodal: 7.8 ± 0.3, 14 ± 2, and 28 ± 10 Å (0.78 ± 0.03, 1.4 ± 0.2, and 2.8 ± 1 nm, respectively). The total pore volume is 0.26 cm^3/g, and the specific volume extrapolated from Eq. (6),

$$\rho = 2 + 1.35[N] \quad (6)$$

where ρ is the density and [N], the measured nitrogen concentration, is 0.5 cm^3/g; thus, one third of the apparent particle volume is porosity. The first two pore-size modes account for 50% of the total pore volume. The corresponding micrograph of the particles is shown in Fig. 8.

The LPSPs are X-ray amorphous, thus limiting structural characterization; however, the nature of the amorphous network can be assessed from DRIFTS studies.[35–38] Infrared (IR) spectroscopy provides information about surface species as well as bulk.[39]

DRIFTS spectra of untreated LPSPs are shown in Fig. 9; the 1300–1400 cm^{-1} region is expanded in the inset. The main absorption bands, the 1094 cm^{-1} peak with a shoulder at 1175 cm^{-1}, are ascribed to threefold degenerate stretching of SiO_4 tetrahedra. The weak shoulder at 975 cm^{-1} is assigned to ν(Si–O) of silanol groups. The weak peak at 812 cm^{-1} is assigned to an Si–O–Si bending mode, and the strong peak at 454 cm^{-1} with a shoulder at 475 cm^{-1} is ascribed to O–Si–O bending. The weak, sharp peak at 3740 cm^{-1} corresponds to ν(O–H) of isolated OH groups, and the two broad peaks at 3200 and 3650 cm^{-1} are associated with hydrogen-bonded ν(OH), e.g., adventitious water.

There are several IR-active surface species that can form via reactions (3)–(5) and Fig. 1—for example, silanol groups (≡Si(OH)), amides (≡Si(NH_2)), and imides (or silazane) (≡Si–NH–Si≡). The bulk consists of a network of $Si(O,N)_4$ subunits with a variety of O:N ratios. Some of the characteristic absorption frequencies taken from the literature are shown in Table I. The peak positions tabulated are taken from materials with long-range periodicity, such as crystalline ceramics and relatively simple, linear polymers. Therefore, the actual peaks in the nitrided LPSP spectra broaden and shift accordingly. Broad peaks are indicative of absorption environments that have a disruption of long-range order, as seen in amorphous materials or materials with distributions in composition, such as tetrahedral $Si(O,N)_4$.

DRIFTS spectra of ammonolyses for 4 h at successive temperatures are shown in Fig. 10. The spectra have features similar to those of amorphous silica,[40] yet they deviate with increasing processing temperature. The spectra show several features: (i) bands at 1200 and 1100 cm^{-1} that occur from threefold degenerate stretching vibrations of the $Si(O,N)_4$ structural unit; (ii) bands centered at 800 and 460 cm^{-1}, due to Si–O–Si and O–Si–O bending vibrations, respectively; and (iii) a shoulder at 970 cm^{-1} indicative of Si–N bending. However, included in this envelope of peaks are contributions from the stretching vibrations of nonbridging Si–O at 960 cm^{-1} resulting from silanol groups.

The changes seen in these spectra are atypical of an amorphous material subjected to these heat treatments. The large free volume associated with pyrolyzed precursors decreases with the extent of annealing. The decrease in free volume manifests an increase in short-range order. Thus, the normal trend for IR absorptions in amorphous materials is a sharpening of peaks with increased processing temperature;[32] however, the broadening observed here is a result of the changes in composition that accompany the temperature change, where nitrogen now occupies some of the oxygen sites. This partial substitution creates envelopes of absorptions about characteristic positions. Thus, the peaks associated with lattice vibrations are broader and shifted (from expected SiO_2 values) to lower wavenumbers (1060 cm^{-1} and broad shoulder) and exhibit relative intensities that reflect increases in nitrogen content with increases in processing temperature.

The high-wavenumber region (4000–1450 cm^{-1}) of the DRIFTS spectra in Fig. 10 shows a decrease in the isolated hydroxyl ν(OH) vibration at 3740 cm^{-1}, with respect to as-processed LPSPs (see Fig. 9). The peaks at 3200 and 3380 cm^{-1} can be assigned to NH stretches. As stated earlier, there are several possible OH and NH species, as well as complexes with physisorbed NH_3, that account for these absorptions. The peak at 1550 cm^{-1} likely results from bending vibrations of NH_2 groups with shoulders at 1540 and 1560 cm^{-1}

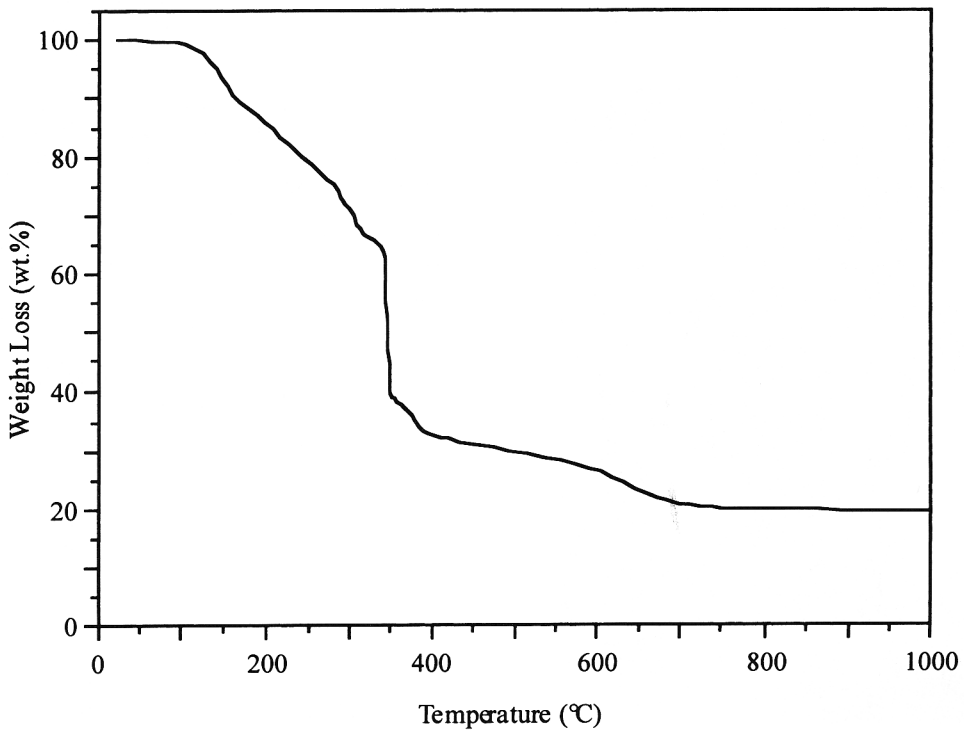

Fig. 6. TGA of silatrane glycolate complex in air (ceramic yield ~20 wt%).

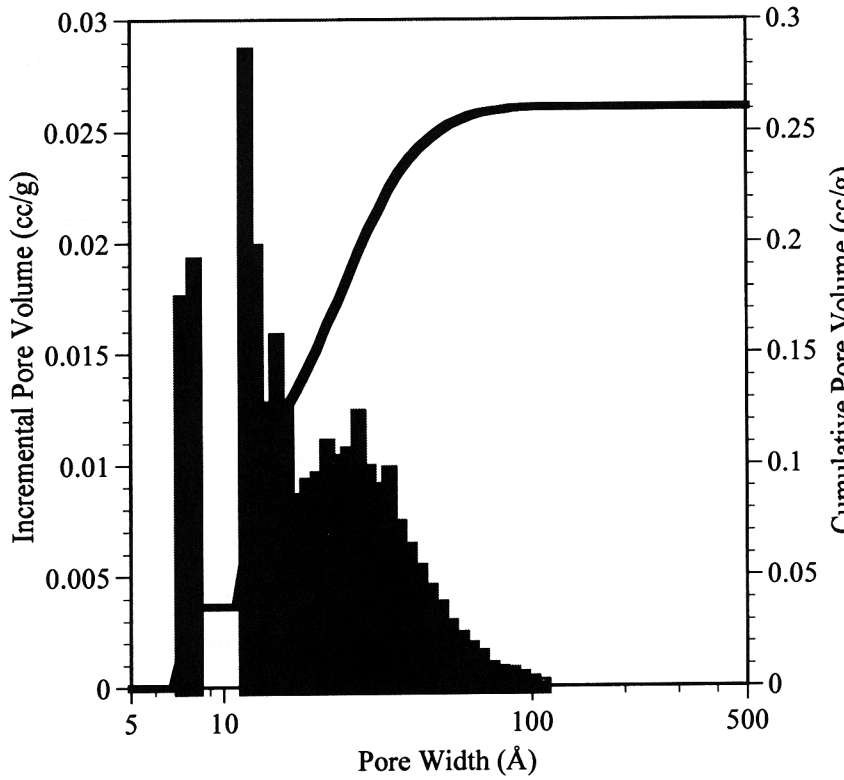

Fig. 7. Pore-size distribution for LPSPs after two-step pyrolysis at 500°C; incremental and cumulative pore volume plotted as a function of pore width.

from related species.[16] The peak at 1400 cm^{-1} is attributed to bending in NH_4^+.[39]

The nitrogen content of LPSPs (4 h of nitridation) is plotted in the Arrhenius format in Fig. 11. An Arrhenius activation energy of 54 kJ/mol was calculated with a preexponential constant of 2900. Nitridation for longer time intervals appears to approach the nitrogen saturation limit of silicon oxynitride (Si_2N_2O) and, therefore, does not follow the same behavior.

The helium pycnometry densities (ρ in Eq. (6)) of LPSPs nitrided in a FBR in 1.5 L/min NH_3 are plotted as a function of the measured nitrogen concentration in Fig. 12. The powder densities increase linearly as temperature increases at a given time and as time increases at a given temperature.

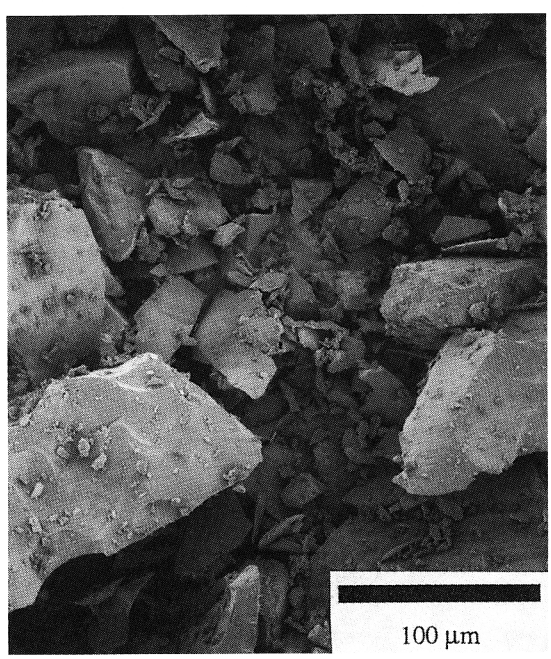

Fig. 8. SEM micrograph of LPSPs as-prepared (500°C).

A plot of the BET SSAs as a function of temperature is shown in Fig. 13. An estimate of diffusion distances can be made by comparing equivalent spherical radii calculated from the SSAs and ρ values. If we assume the particles are spherical, we can derive a worst-case diffusion distance. Initially, the LPSPs have a density of 2.0 g/cm^3, a SSA of 525 m^2/g, and a worst-case diffusion distance of 2.9 nm; whereas, after nitridation at 1000°C for 4 h, the SSA value of 300 m^2/g and ρ value of 2.17 g/cm^3 give a worst-case final diffusion distance of 4.6 nm. The marked decrease in SSA between 800° and 900°C is likely the onset of sintering of the internal porosity. Very importantly, recall that the external surfaces only negligibly influence the SSA.

Entrainment of powder has the effect of classifying the nitrided LPSPs, as evident in the SEM micrograph shown in Fig. 14. The figure shows large particles similar to Fig. 8, yet with minimal evidence of fine particles. The particles have similar texture, with no evidence of grain formation or vapor-deposited growths.

Nitrogen concentrations plotted against time for processing at 900° and 1000°C are shown with saturation curves fitting

$$[N] = N_0^*[1 - \exp(-t/\tau)] \quad (7)$$

where N_0 = 20 and 20.5 wt% and τ = 6.5 and 3.8, respectively, in Fig. 15. The saturation constant is less than the expected 28 wt% for Si_2N_2O. The average hydrogen content by chemical analysis, over all the 4 h data, is 0.71 ± 0.14 wt%. No correlations are evident between measured hydrogen content and processing time or temperature.

XRD of LPSPs as processed and nitrided at 1000°C for 24 h appears in Fig. 16. The main feature is due to scattering by tetrahedral $Si(O,N)_4$. The pattern from the nitrided powder is broader and skewed toward higher 2θ values than the as-processed LPSPs.

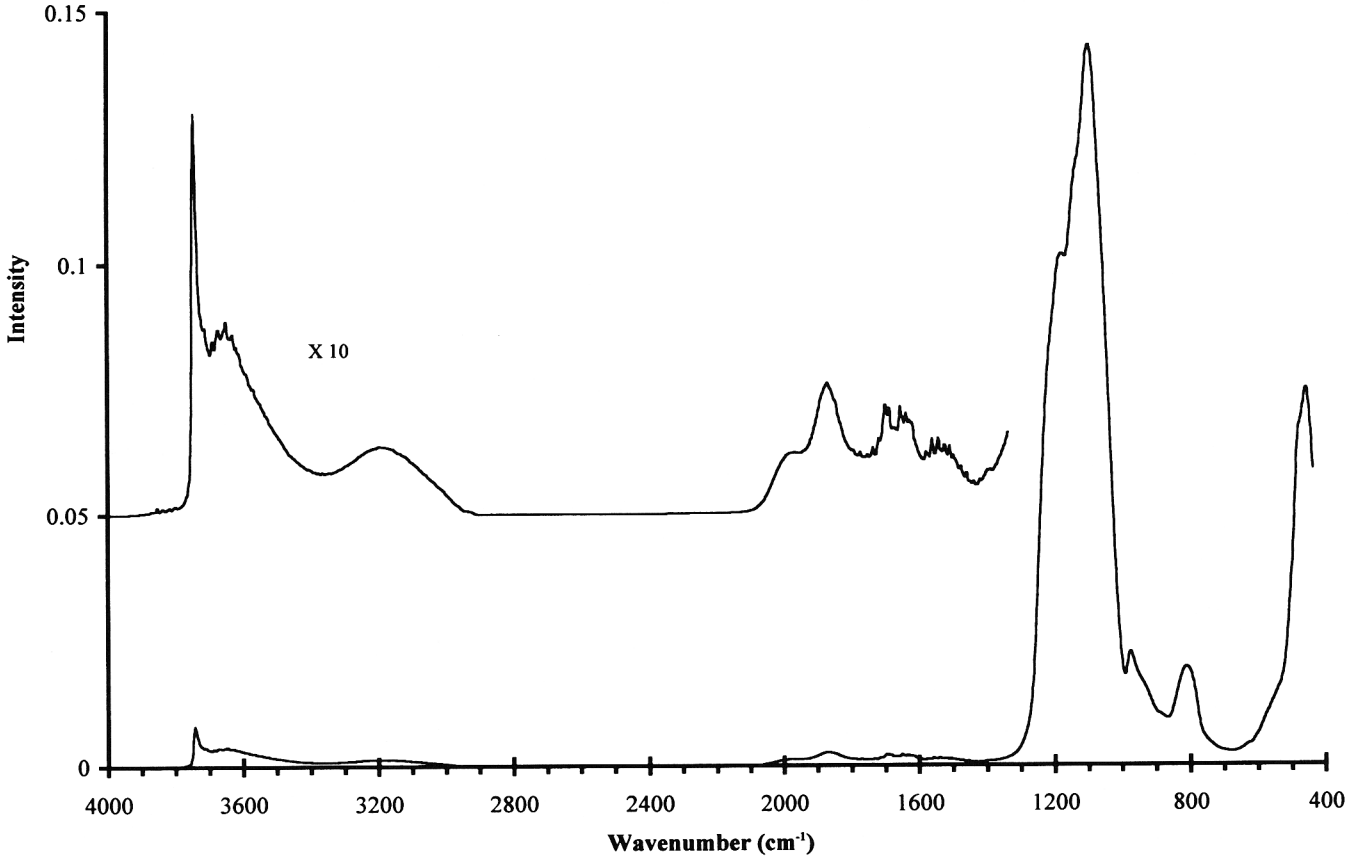

Fig. 9. DRIFTS spectra of untreated LPSPs (inset expanded 10×).

XPS data was compared to that in the literature[44–47] to provide additional characterization of the nitrided materials. The data tabulated in Table II are presented in terms of binding-energy differences for a sample nitrided at 1000°C for 4 h with an NH_3 flow rate of 1.5 L/min. Evaluating the data by means of binding-energy differences, rather than absolute values, minimized ambiguities in absolute energies stemming from charge buildup common to ceramics. The binding energies measured were for the Si-2*p*, O-1*s*, and the N-1*s* photoelectrons. The sample was analyzed as nitrided (unground) and following a postnitridation grinding with a mortar and pestle (ground). The purpose was to compare the binding states of the outermost surfaces with those of surfaces exposed by grinding. The pores were assumed to act as critical flaws during grinding such that pore surfaces would be exposed on grinding. The values found (Δ(Si,N) = 295.2–295.5 eV) are in good agreement with those of crystalline Si_2N_2O (295.6–295.7 eV). Furthermore, the data for the ground and unground samples show no significant differences.

IV. Discussion

The primary objectives of the model study described here were to examine the utility of processing nitrided glasses using highly porous powders derived from polymer precursors and to develop a well-defined fluidized-bed process for nitridation. In the following sections, we briefly discuss the synthesis of the silatrane glycolate precursor, the methods developed for the production of LPSPs from this precursor, and our efforts to define an optimum set of parameters for processing high-nitrogen-content oxynitride amorphous powders.

Table I. Characteristic Infrared Absorption Frequencies for Si–N and Si–O Moieties

Peak position (cm^{-1})	Absorption mode	Reference
475	O–Si–O Bending	40
800	Si–O–Si Bending	39, 40
850–900	Si–N–Si	41
900	Si–NH–Si asymmetric stretch from bridging silazane	16
932, 938	Si–NH_x from silylamine and disilazane groups	16
960	Si–O, nonbridging Si–O such as silanol	40, 42
1170	N–H imide bend	43
1200, 1100	Threefold degenerative stretching of SiO_4 tetrahedra	39, 40
1550 and shoulders	Geminal $Si(NH_2)_2$	16
1840	Lattice combination vibration	16
3200	Molecular water	39
3333	–NH stretching vibrations	12
3380	–NH stretching vibrations arising from silamine (Si–NH_x)	42
3508	OH stretch	12
3740	Free hydroxyl or isolated silanol groups	39

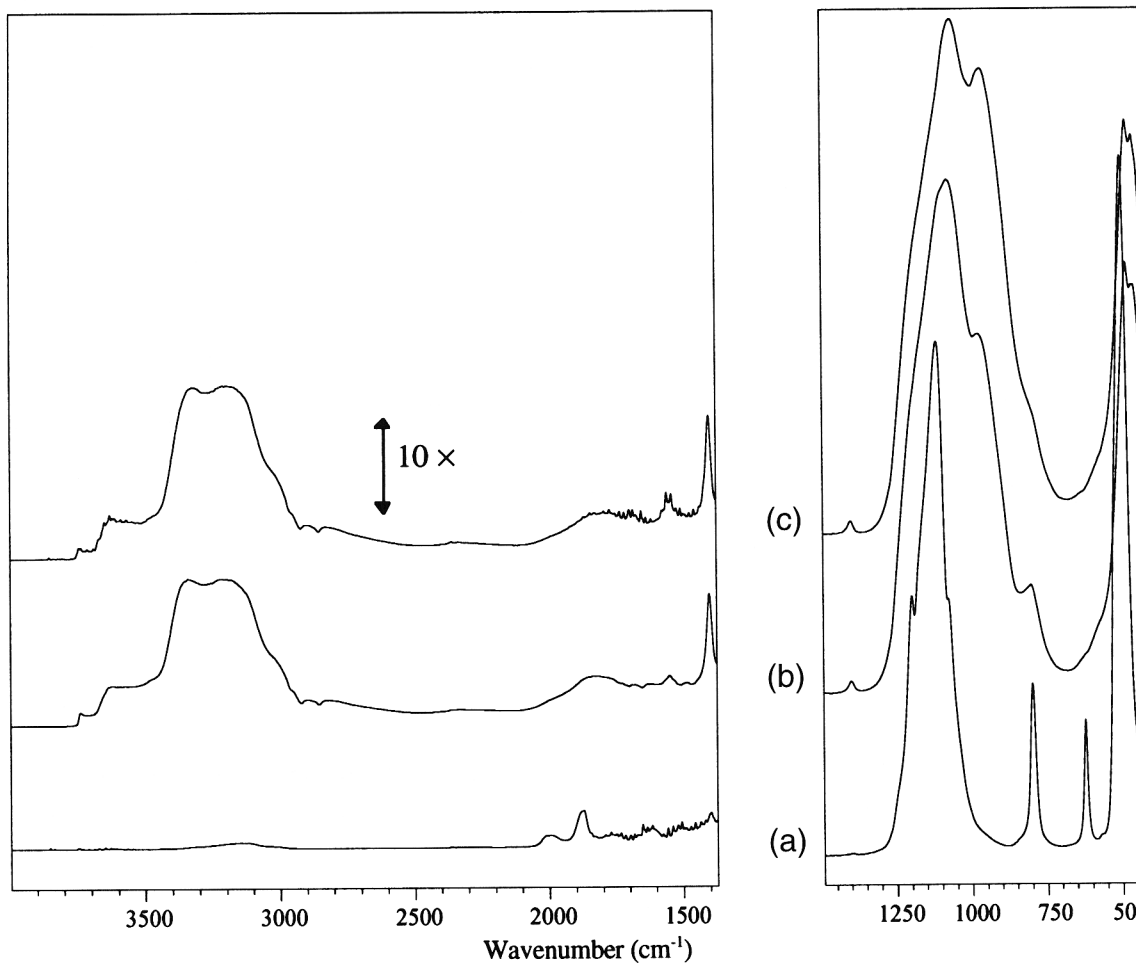

Fig. 10. DRIFTS spectra of LPSPs nitrided for 4 h at (a) 800°, (b) 900°, and (c) 1000°C by ammonolysis in a FBR. Intensities are in Kubelka-Munk units, and the 4000–1450 cm^{-1} region is 10× the 1500–400 cm^{-1} region.

(1) Synthesis

Inexpensive, high-ceramic-yield precursors are key to developing economically viable chemical routes to ceramics. Thus, our recent discovery of the direct synthesis of silatrane glycolate from silica, TEA, and EG (Fig. 4) provides significant motivation for examining its use as a ceramic precursor.[34] In this study, the silatrane glycolate was synthesized using fumed silica as the silicon source; however, the same reactions can be conducted with inexpensive silica sources including beach sand, fused silica, and diatomaceous earth.[34,48–50]

(2) Powder Preparation: Pore Development via Pyrolysis

A processing window for bulk pyrolysis was developed by combining information from TGA with our goal of producing a high-SSA, low-carbon-content powder. The viscosity of the precursor solution is a function of temperature and EG concentration. Increases in precursor viscosity have important consequences on microstructural and pore development. As the viscosity increases during pyrolysis, transport of volatiles from interior regions is inhibited, resulting in nucleation and growth of gas bubbles. As the polymer/EG mixture is further heated, any remaining EG will contribute to the gaseous expansion and will foam the viscoelastic polymer. Polymer solvation by the residual EG will further aid in the swelling process. This combination of pressurization and swelling can result in large volume expansions and leave a highly porous, foamed structure. At this point, the porous structure is a polymer network strained by the pressurized pores and will collapse from surface tension if heat (i.e., pressure source) is removed prior to the polymer being rendered infusible. The porous structure can be retained by heating rapidly through decomposition.

Pyrolysis forms the metal oxide structure, volatile organic products, and pyrolytic carbon. Processing conditions for bulk pyrolyses greatly affect powder properties. In particular, the SSAs of powders were markedly different based on heating schemes. Higher SSAs were obtained when samples were placed in a furnace preheated to 500°C (525 m^2/g) than when samples were ramped at 10°C/min to 500°C (250 m^2/g). The advantage of preheating over ramping is that sufficient thermal energy is available to induce polymerization and decomposition reactions in the material while sufficient EG vapor is present to foam the polymer.

Additionally, greater porosity was exhibited in powders pyrolyzed in flowing N_2 rather than flowing air, presumably because greater elasticity is retained in the polymer when it does not undergo coincidental oxidative crosslinking. This elasticity is essential to precursor swelling and is only present while the precursor has polymeric behavior. In contrast, decomposition in air can oxidize (crosslink) the polymer ligands, eliminating viscoelastic properties. Moreover, the gases from oxidized ligands will not aid viscoelastic expansion by polymer solvation. Thus, pyrolysis in N_2 promotes the development of porous ceramic powders, albeit without providing oxidation of pyrolytic carbon.

Following the N_2 isothermal pyrolysis, the resulting material was ground to provide flowable powders and then subjected to an additional isothermal pyrolysis in O_2 to remove residual carbon. Carbon removal was performed through oxidative isothermal treatments above the decomposition temperature, with higher temperatures resulting in faster rates. The optimal temperature was determined by monitoring the SSA, pore-size distribution, and carbon content as functions of processing temperature. A balance of carbon removal and pore development

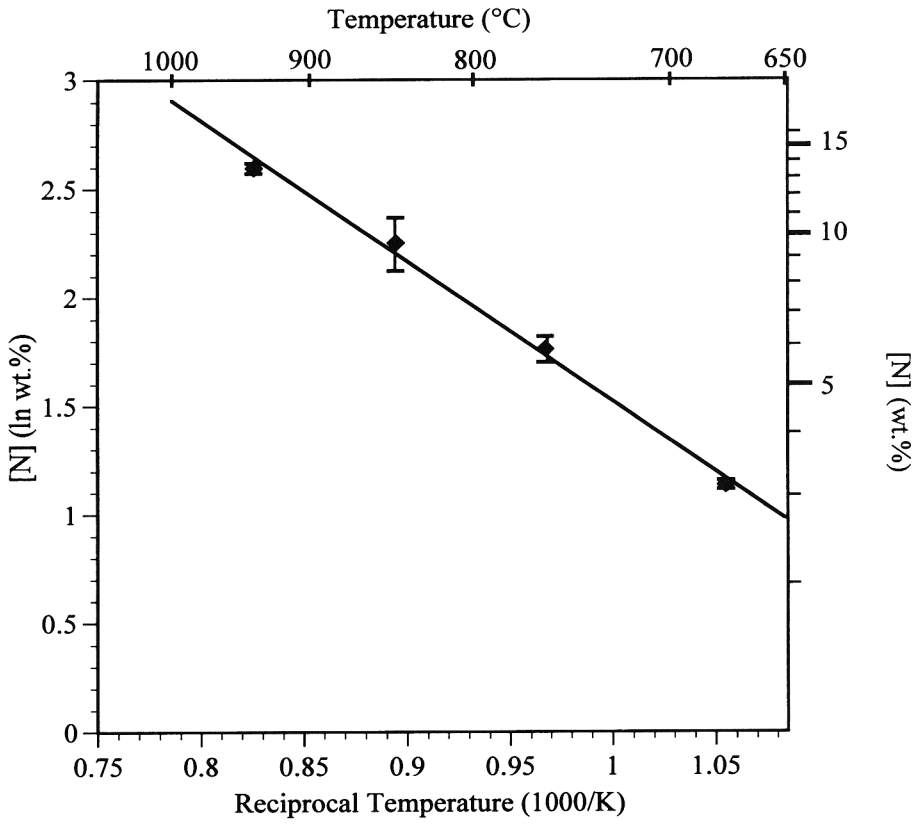

Fig. 11. Nitrogen content of LPSPs as a function of nitridation temperature for powders in a FBR for 4 h in 1.5 L/h NH_3. Data are averages of at least two runs (±7%).

was achieved for pyrolyses conducted at 500°C, resulting in a light-colored, low-carbon ([C] < 1 wt%), high-SSA (525 m^2/g) powder. Flowable powders are necessary for fluidization and were obtained by grinding and classifying the pyrolyzed precursor powders (−100 mesh). The large particle size (<150 μm) was chosen to reduce the effects of electrostatic agglomeration, which inhibits flowability. The drawback to the large size is longer diffusion distances through the pore network for the gaseous reactants and products, which increases the time required for oxidation and ammonolysis. The ground powders

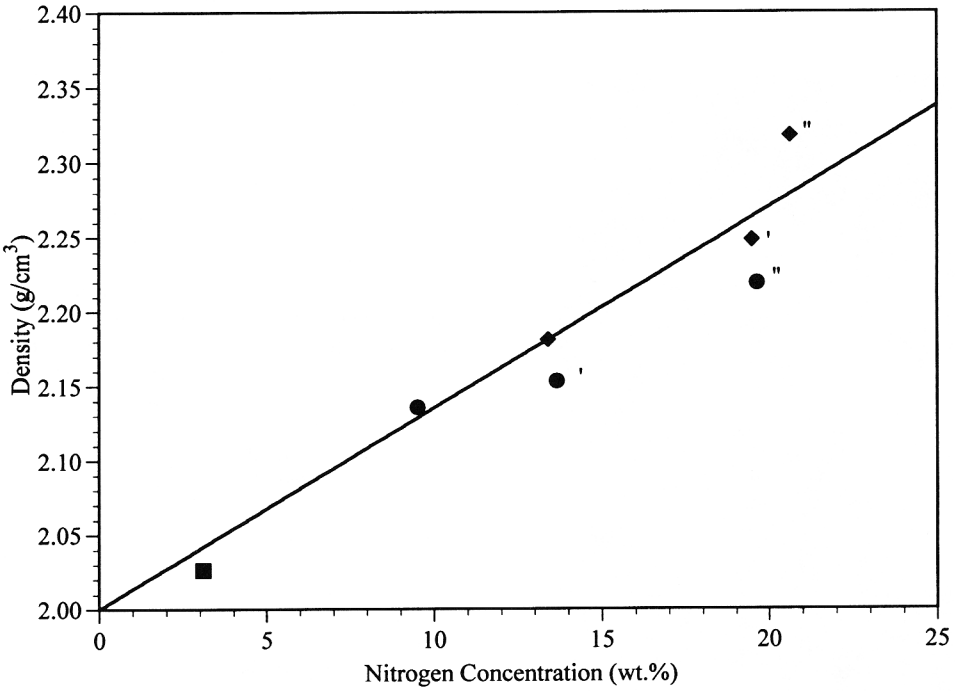

Fig. 12. Pycnometric densities of LPSPs nitrided in a FBR in 1.5 L/min NH_3 plotted as a function of measured nitrogen concentration. Data are averages of two or more runs (±5%) for temperatures of (■) 700°, (●) 900°, and (◆) 1000°C, and times of 4, 12 (marked with a single prime, ′), or 24 h (marked with a double prime, ″).

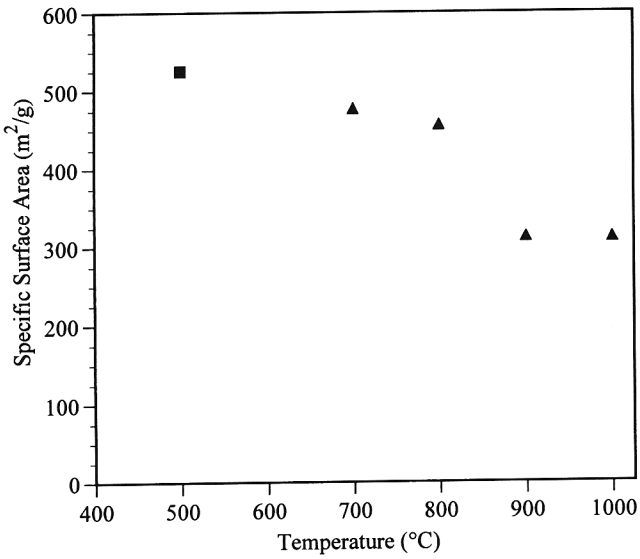

Fig. 13. BET analysis of LPSPs nitrided in a FBR for 4 h in 1.5 L/h NH_3. Plotted are the (■) oxidized and (▲) nitrided powders.

were oxidized in a fixed-bed regime, where the flow rate was adjusted periodically to eliminate channeling.[30]

Rapid pyrolysis of the precursor in N_2 followed by oxidation results in a porous material. The porosity can be classified into two pore types, as seen in the pore-size distribution (Fig. 7): the first type consists of two narrow distributions, whereas the second type is a broad mesoporous distribution. A model to describe this pore distribution follows. During pyrolysis, a solution forms that contains a nonequilibrium mass of reactive species; therefore, many of the solution precipitation concepts should apply, where a nucleus forms and continues to grow into a three-dimensional interconnected molecular network. The domains that form from each nucleus continue to grow until the reactants are consumed or abutment with another domain occurs. The structures of these domains can simply be the interconnecting lattice as described by Scherer[51] and also Brinker and Scherer[52] and would give well-defined pore structures, as seen in the first type. The second smooth, broad, mesopore distribution is indicative of interdomain pores. The high porosity provides a large reaction surface for ammonolysis.

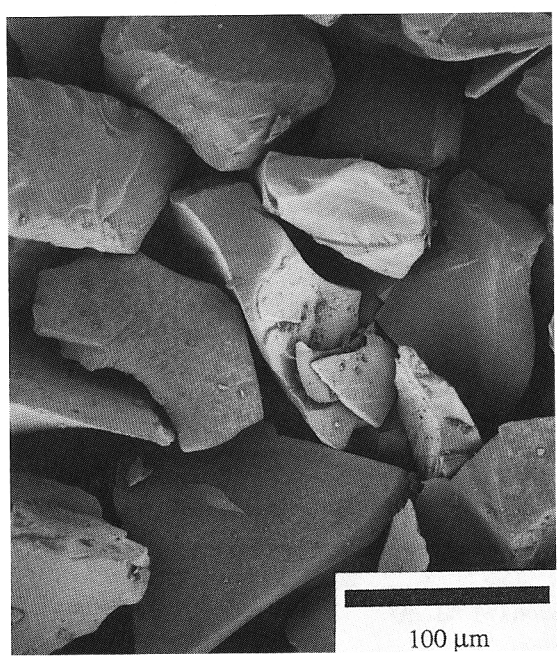

Fig. 14. SEM micrograph of LPSPs nitrided in a FBR at 1000°C for 12 h in 1.5 L/h NH_3.

(3) Nitridation

The nitridation scheme we envison is transport of NH_3 to the particle surface, gas/solid reaction at the surface, and diffusion of nitrogen species in the bulk. Ammonolysis is a gas/surface interface reaction and occurs readily at the temperatures studied. IR studies and chemical analysis provide evidence of the reactions depicted in Fig. 1 at all the temperatures studied. We make the assumption that the near surface becomes saturated in a short time; therefore, viewing the nitridation process as a constant composition surface that is diffusion limited is best. These constraints are the motivation for developing amorphous powders with high SSAs. Additionally, ammonolysis requires continual exchange of gaseous species (the reacting gas (NH_3) and the reaction byproduct (H_2O), reaction (2)), which leads to concentration gradients in the gas that can result in a heterogeneous distribution of nitrogen in the product. An initial ammonolysis study with flow over a fixed bed confirmed the dependence of nitrogen contents on flow rate. Nitrogen contents increased as the flow rate increased, until a local maximum was achieved, and values tailed off with further increases in flow rates. Heterogeneous powder beds resulted in these experiments, with higher nitrogen contents for powder near the surface of the bed.

An ammonolysis technique was sought wherein homogeneous powders would be inherent by design, e.g., a FBR. One advantage of a fluidized system is that overfluidization, although inefficient, does not result in heterogeneous powders. To ensure against channeling or dead zones, the flow rate for full fluidization was set at ambient temperature. Thus, as the gas expands with temperature, there is an increase in the flow rate. The increase in flow rate beyond full fluidization entrains fine particles and is evidenced by the lack of fine particles in the SEM micrograph shown in Fig. 14. Fluidized-bed reaction of LPSPs has two main advantages: (i) the length of percolation of NH_3 is minimized to the scale of the particle, as opposed to the depth of the powder bed for fixed-bed reactions of finer particles, and (ii) homogeneity is maintained in the powder bed by the stirring action of the fluid.

The temperature effects of nitridation were studied to develop an understanding of the nitridation process. An activation energy of 54 kJ/mol was calculated from the data in Fig. 11. Wusirika[17] reports an activation energy for nitridation (76 kJ/mol) that compares to the diffusion of several species in silica (water, 72 kJ/mol; hydrogen, 37 kJ/mol; and nitrogen, 109 kJ/mol). The Wusirika experiments were conducted in dynamic flow (10 L/min in a 2 L furnace) over a bed of powder (fumed silica, 180 m^2/g, d = 14 nm). Furthermore, the Wusirika calculations separate the NH_3 partial pressure dependence and time from the preexponential term; thus, the nitrogen content in the silica exhibits a linear dependence on the NH_3 partial pressure and a square-root dependence on time. The conclusion is that a diffusion mechanism is the rate-limiting process. Although there are significant differences in the experimental design, these results are quite reasonable and served as a foundation for our experimental design.

The lower activation energy in our study can be attributed to transport-limited phenomena that diminish thermal effects. The extensive porosity of LPSPs provides an increase in reaction surfaces available; however, the pore widths are quite small (<100 Å (<10 nm)) and restrict gas flow. Because of the small pore sizes, transport of gaseous reactants and products to/from the reaction sites of internal pore surfaces is likely to limit the rate of ammonolysis. Gas transport in this environment is likely to be in the Knudsen flow regime and, therefore, would be negligibly influenced by thermal activation.

A second mass-transport limitation is homogenization of nitrogen by diffusion in the bulk phase. Nitrogen diffuses slowly at the low-to-moderate temperatures used in the studies

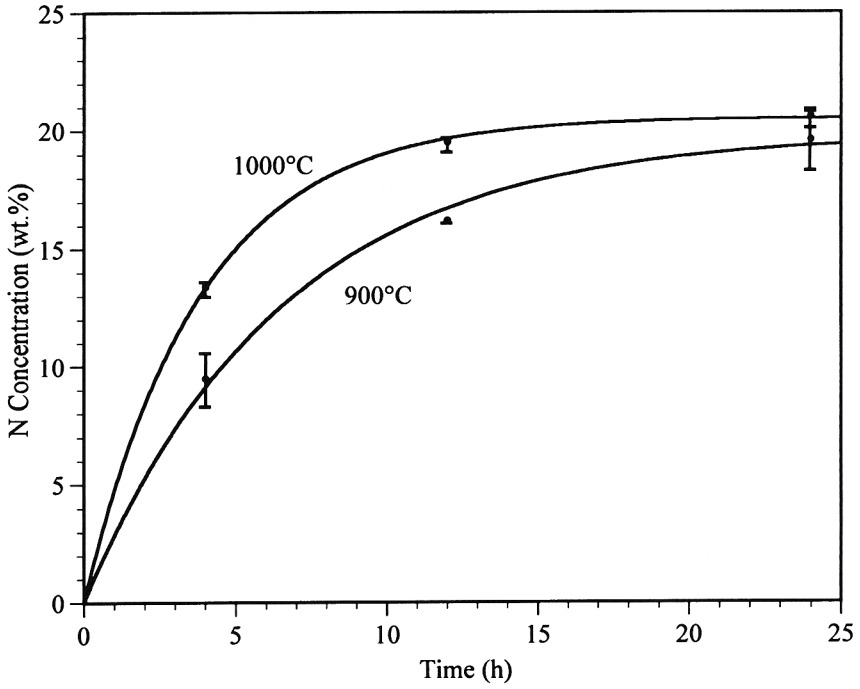

Fig. 15. Chemical analysis of LPSPs nitrided in a FBR at 900° and 1000°C in 1.5 L/h NH_3. Data points represent the averages and standard deviations of several determinations.

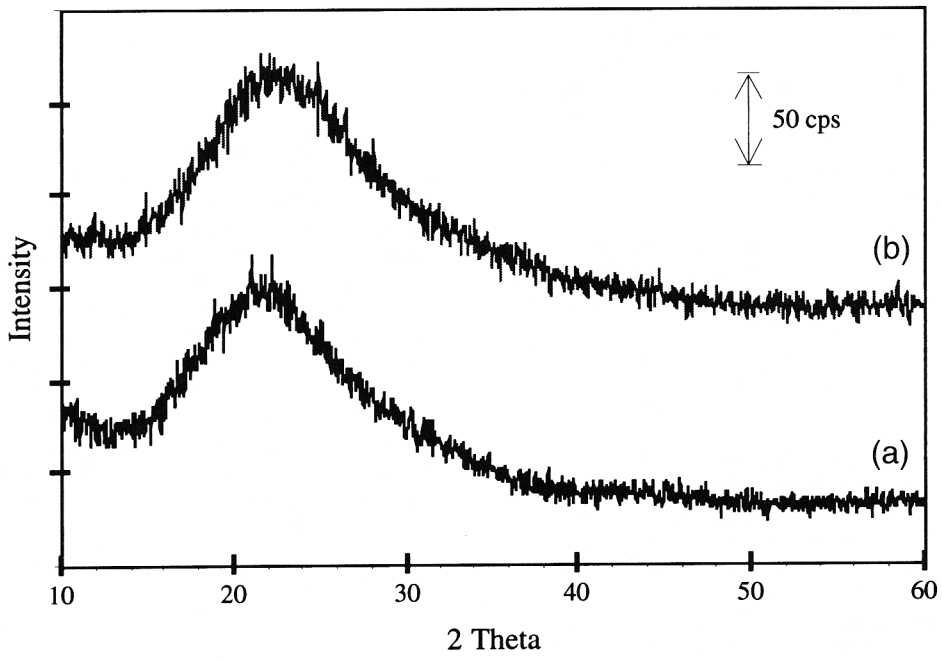

Fig. 16. Powder XRD of LPSPs (a) as processed and (b) nitrided at 1000°C for 24 h.

Table II. Binding-Energy Differences (eV) for Nitrided LPSPs*

Sample condition†	Δ(Si-2*p* − O-1*s*)	Δ(O-1*s* − N-1*s*)	Δ(Si-2*p* − N-1*s*)
Unground	430.0	134.5	295.5
Ground	430.1	134.9	295.2
Si_2N_2O[47] (1120°C, 4 h)	429.8	134.5	295.3
Si_2N_2O[47] (1120°C, 24 h)	430.0	134.6	295.4
Si_2N_2O[46]			295.6
Si_3N_4[46]			295.7
Si_2N_2O[46]	430.0	134.5	295.5
Silica glass[46]	427.6		
Quartz[46]	430.6		

*LPSP nitrided in a fluidized-bed reactor at 1000°C for 4 h in 1.5 L/min NH_3. †Superscripts denote reference source.

described here; therefore, avoiding homogenization by bulk diffusion is necessary. Fortunately, the potential problems associated with slow bulk diffusion can be partially resolved by retaining high SSAs during nitridation. Surface reactions become the dominating factor under this hypothesis, with bulk homogenization becoming rate limiting on surface saturation. Powders examined by DRIFTS show the surface species expected for the reactions shown in Fig. 1, where a decrease in silanol groups, with a concurrent increase in amine groups, indicates progression through the reaction series. These surface reactions form Si–$(NH_x)_y$ groups and are highly dependent on the partial pressure of water, thus requiring the exchange of gaseous reactants and products as stated above.

Homogenization is highly dependent on the mobility of the diffusing species. The mobility is a function of the driving force, the mobile species, and the lattice. As concentration gradients decrease, the driving force for further diffusion decreases, and homogenization rates decrease correspondingly. Habraken *et al.*[53] suggest that the NH_x species, rather than atomic nitrogen, diffuse, and a portion of the nearly constant hydrogen content seen in these studies can be attributed to silazane groups in the bulk as well as at surfaces.

The mobility of the diffusing species also is greatly affected by the free volume in the glass. Densities increase as the processing increases, thus potentially lowering the free volume and, hence, lowering the mobility. Many parameters in the system change with processing, thus limiting the conclusions that can be made in regard to diffusion rates or mechanisms.

Saturation of the nitrogen content of LPSPs appears to occur at ~21 wt% for processing at 1000°C, as seen in Fig. 15. Thermodynamic studies[45] on the nitridation of amorphous silica gel suggest that the nitrogen concentration should approach a composition equivalent to Si_2N_2O (28 wt% nitrogen 40 at.%) at 1000°C. The calculations justify the driving force for nitridation; however, the enthalpy of crystallization to Si_2N_2O does not aid the process, because the materials remain amorphous. Additionally, the low saturation limit is influenced by the single mechanism assumed for the model (Eq. (7)). However, nitridation rates are strongly influenced by surface reactions, where reactions similar to those shown in Figs. 1(a) and (b) deplete the surface of silanol groups in favor of NH_x (compare DRIFTS spectra in Figs. 9 and 10(a)). At later stages, nitridation must proceed via bulk diffusion, which likely occurs at a slower rate. Thus, a model that incorporates the slower bulk diffusion step may better describe the latter stages of nitridation.

Van Weeren *et al.*,[47] in studies on the ammonolysis of silica gel, observed that a composition similar to that of Si_2N_2O was obtained after extended periods. However, solid-state nuclear magnetic resonance (NMR) indicated the presence of all five $SiO_{4-x}N_x$ species, with a global composition approaching that of Si_2N_2O. No evidence for the formation of Si_2N_2O was observed, implying that Si_2N_2O does not really form during nitridation, as predicted on thermodynamic grounds.[45] They suggest that nitridation may only slow down as the composition approaches Si_2N_2O. One reason may be that the silica surface is fully transformed to silicon nitride (Si_3N_4) and no oxygen remains to be replaced. Hence, only by bulk diffusion will equilibration bring oxygen back to the surface such that further nitridation can occur. Based on kinetic arguments alone, Si_3N_4 should be the final phase formed. The question of whether it is more stable than Si_2N_2O in a nitriding environment, where crystallization of Si_2N_2O does not occur, remains to be proven.

The uniformity in the XPS data (Table II) indicates that reactions occur on the interior pore surfaces, which implies that transport of NH_3 and H_2O across the boundary layer of the fluidized particles occurs readily. Similarly, transport of these species through the porous network also occurs. Comparison of the powder XRD patterns also corroborates the incorporation of nitrogen, where the skewing of the X-ray peak toward higher 2θ is attributed to the various statistical combinations of $Si(O,N)_4$.[17] The five separate $Si(O,N)_4$ tetrahedral environments have all been observed by solid-state ^{29}Si NMR.[47]

Given that large-scale viscous flow was not encountered in these nitridation studies, the decrease in surface area with increases in processing can be attributed to the loss of porosity. More importantly, the loss of porosity appears to proceed without pore entrapment, because a linear increase in ρ was observed with processing. Helium pycnometry measures the specific volume of the material accessible to helium; therefore, it is a measure of the apparent density of a material. If the loss in pore area observed by BET was due to pore entrapment, an increase in specific volume as a function of processing would be expected, i.e., lower apparent density. This finding is critical to the overall purpose of this research. If pore closure were predominant during sintering, the material would be rendered useless as a precursor to monoliths or fibers. The increase in density with processing then can be attributed to a combination of the compositional change (oxide to oxynitride) as well as the loss of free volume with processing (annealing).[52]

Fluidized-bed reactions of LPSPs appear to be a viable technique for synthesis of silicon oxynitride powders and may be a general method of nitriding aluminosilicates as well. The significance of reducing diffusion distances must be reiterated. Because chemical reactions and diffusion are thermally activated processes, the energy added to sustain diffusion may be too great, thus inducing glass decomposition reactions, e.g., reactions (1) and (2). Nitriding LPSPs appears to provide access to the same materials with lower processing temperature requirements than melt processing, thereby minimizing potential problems. This is accomplished by creating a high-SSA material, although the cost of doing so is lengthy gas-diffusion distances resulting because of the tortuous porous pathways. The thermal stability of these porous powders may be useful themselves as supports in filtration or catalysis.

V. Summary

Silatrane glycolate provides ready access to large, porous, silica particles (LPSPs) via a two-step isothermal pyrolysis process. The first step—pyrolytic decomposition in nitrogen—generates a highly desirable porous powder that contains mesopores as well as micropores. The second step oxidatively removes residual organics and pyrolytic carbon. The LPSPs have high specific surface areas because of internal porosity. Nitridation of LPSPs in a fluidized-bed reactor produces amorphous oxynitride powders with high nitrogen content (up to 21 wt%). The Arrhenius activation energy for nitridation has been calculated to be 54 kJ/mol. This activation energy is lower than previous work and is likely due to mass-transport limitation in the vapor phase, as opposed to the bulk phase.

Powder density measurements show increases in density that can be directly correlated with increases in nitridation times and temperatures. Densification correlates with nitrogen content and indicates that the contraction of the crosslinked network occurs as a result of nitrogen substitution for oxygen. X-ray photoelectron spectroscopic characterization of the powders has established that binding-energy differences are similar to those reported for silicon oxynitride and that the nitridation process extends into the interior surfaces. This study serves as a model for nitridation of multicomponent glasses, which will be described in forthcoming papers.

References

[1]D. R. Messier and R. P. Gleisner, "Mg-Si-Al Oxynitride Glasses," U.S. Army Materials Technology Laboratory, MTL TR 92-6, February 1992, and references therein; see Ref. 2.

[2]P. F. Aubourg, "Melt Processing Based on the Composition of 'S' Glass (15.5 mol% Al_2O_3, 15.5 mol% MgO, 69 mol% SiO_2), with Substitution of Si_3N_4 for SiO_2 (15.49 mol% Al_2O_3, 15.49 mol% MgO, 62.02 mol% SiO_2, 7.00 mol% Si_3N_4)"; personal communication.

[3]K. H. Jack, "Review. Sialons and Related Nitrogen Ceramics," *J. Mater. Sci.*, **11**, 1135–58 (1976).

[4]R. E. Loehman, "Oxynitride Glasses"; pp. 119–49 in *Treatise on Materials Science and Technology*, Vol. 26. Edited by M. Tomozawa and R. H. Doremus. Academic Press, New York, 1985.

[5]S. Sakka, "Oxynitride Glasses," *Annu. Rev. Mater. Sci.*, **16**, 29–46 (1986).

[6]T. Ekström and M. Nygren, "SiAlON Ceramics," *J. Am. Ceram. Soc.*, **75** [2] 259–76 (1992).
[7]P. Kansal, "Novel Chemical Routes to Ceramics from Precursors"; Ph.D. Dissertation. University of Michigan, Ann Arbor, MI, January 1996.
[8]J. Homeny and D. L. McGarry, "Preparation and Mechanical Properties of Mg-Al-Si-O-N Glasses," *J. Am. Ceram. Soc.*, **67** [11] C-225–C-227 (1984).
[9]J. Mukerji, P. K. Das, and D. Chakraborty, "Properties of Glasses and Melts in the System MgO–AlN–SiO_2," *Am. Ceram. Soc. Bull.*, **66** [11] 1616–19 (1987).
[10]J. Homeny, G. G. Nelson, S. W. Paulik, and S. H. Risbud, "Comparison of the Properties of Oxycarbide and Oxynitride Glasses," *J. Am. Ceram. Soc.*, **70** [5] C-114–C-116 (1987).
[11]W. K. Tredway and S. H. Risbud, "Multianion Glasses"; pp. 203–12 in *Non-oxide Technical and Engineering Ceramics*. Edited by S. Hampshire. Elsevier, New York, 1986.
[12]H. O. Mulfinger, "Physical and Chemical Solubility of Nitrogen in Glass Melts," *J. Am. Ceram. Soc.*, **49** [9] 462–67 (1966).
[13]C. J. Brinker, "Formation of Oxynitride Glasses by Ammonolysis of Gels," *J. Am. Ceram. Soc.*, **65** [1] C-4–C-5 (1982).
[14]C. J. Brinker and D. M. Haaland, "Oxynitride Glass Formation from Gels," *J. Am. Ceram. Soc.*, **66** [11] 758–65 (1983).
[15]C. J. Brinker, D. M. Haaland, and R. E. Loehman, "Oxynitride Glasses from Gels and Melts," *J. Non-Cryst. Solids*, **56**, 179–84 (1983).
[16]P. Fink, B. Müller, and G. Rudakoff, "Ammoniation and Nitridation of Highly Disperse Silica," *J. Non-Cryst. Solids*, **145**, 99–104 (1992).
[17]R. Wusirika, "Reaction of Ammonia with Fumed Silica," *J. Am. Ceram. Soc.*, **73** [10] 2926–29 (1990).
[18]J. Sjöberg and R. Pompe, "Nitridation of Amorphous Silica with Ammonia," *J. Am. Ceram. Soc.*, **75** [8] 2189–93 (1992).
[19]M. Sekine, S. Katayama, and M. Mitomo, "Preparation of Silicon Oxynitride Glass Fibers by Ammonolysis of Gels," *J. Non-Cryst. Solids*, **134**, 199–207 (1991).
[20]J. Sappei, D. Goeuriot, F. Thevenot, P. L'Haridon, J. Guyader, and Y. Laurent, "Nitridation of γ-Alumina with Ammonia," *Ceram. Int.*, **17** [3] 137–42 (1991).
[21]W. R. Schmidt, V. Sukumar, W. J. Hurley Jr., R. Garcia, R. H. Doremus, and L. V. Interrante, "Silicon Nitride Derived from an Organometallic Polymeric Precursor: Preparation and Characterization," *J. Am. Ceram. Soc.*, **73** [8] 2412–18 (1990).
[22]G. T. Burns and G. Chandra, "Pyrolysis of Preceramic Polymers in Ammonia: Preparation of Silicon Nitride Powders," *J. Am. Ceram. Soc.*, **72** [2] 333–37 (1989).
[23]R. K. Brow and C. G. Pantano, "Composition and Chemical Structure of Nitrided Silica Gel," *Mater. Res. Soc. Symp. Proc.*, **32**, 361–67 (1984).
[24]B. G. Durham, M. J. Murtha, and G. Burnet, "Si_3N_4 by the Carbothermal Ammonolysis of Silica," *Adv. Ceram. Mater.*, **3** [1] 45–48 (1988).
[25]C. Han, "Diphasic Processing of Cordierite," Ph.D. Dissertation. University of Washington, Seattle, WA, 1990.
[26]J. Zarzicki (translated from Fr. by W. D. Scott and C. Massart), *Glass and the Vitreous State*. Cambridge University Press, Cambridge, U.K., 1992.
[27]P. Hrma, "Batch Melting Reactions" (Ch. 5); in *Chemistry of Glasses*, 2d ed. Edited by A. Paul. Chapman and Hall, New York, 1990.
[28]W. D. Kingery, H. K. Bowen, and D. R. Uhlmann, *Introduction to Ceramics*, 2d ed. Wiley, New York, 1976.
[29]J. S. Reed, *Introduction to Ceramic Processing*, 2d ed.; Chs. 17–20. Wiley, New York, 1995.
[30]D. Geldart, *Principles of Powder Technology*; Ch. 6. Edited by M. J. Rhodes. Wiley, New York, 1990.
[31]M. W. Urban and J. L. Koenig, "Recent Developments in Depth Profiling from Surfaces Using FT-IR Spectroscopy" (Ch. 3); in Vibrational Spectra and Structure: A Series of Advances, Vol. 18, *Applications of FT-IR Spectroscopy.* Edited by J. R. Durig. Elsevier, New York, 1990.
[32]P. H. Gaskell, "Models for the Structure of Amorphous Solids" (Ch. 4); in *Materials Science and Technology, A Comprehensive Treatment: Glasses and Amorphous Materials*, Vol. 9. Edited by R. W. Cahn, P. Haasen, E. J. Kramer, and J. Zarzycki. VCH, New York, 1991.
[33]D. L. Pavia, G. M. Lampman, and G. S. Kriz Jr., *Introduction to Spectroscopy: A Guide for Students of Organic Chemistry.* Saunders College Publishing, Orlando, FL, 1979.
[34](a) R. M. Laine, B. M. Mueller, and T. Hinklin, "Neutral and Mixed Neutral/Anionic Polymetallooxanes," U.S. Pat. No. 5 418 298, May 23, 1995. (b) R. M. Laine, D. R. Treadwell, B. L. Mueller, C. R. Bickmore, K. F. Waldner, and T. Hinklin, "Processable Aluminosilicate Alkoxide Precursors from Metal Oxides and Hydroxides. The Oxide One Pot Synthesis (OOPS) Process," *J. Chem. Mater.*, **6**, 1441–43 (1996).
[35]T. K. Trout, J. M. Bellama, F. E. Brinckman, and R. A. Faltynek, "Fourier Transform Infrared Analysis of Ceramic Powders: Quantitative Determination of Alpha, Beta, and Amorphous Phases of Silicon Nitride," *J. Mater. Res.*, **4** [2] 399–403 (1989).
[36]N. Wada and S. A. Solin, "Raman and IR Absorption Spectroscopic Studies on α, β, and Amorphous Si_3N_4," *J. Non-Cryst. Solids*, **43**, 7–15 (1981).
[37]A. Tsuge, Y. Uwamino, T. Ishixuka, and K. Suzuki, "Quantitative Analysis of Powdery Sample by Diffuse Reflectance Infrared Fourier Transform Spectrometry: Determination of the α-Component in Silicon Nitride," *Appl. Spectros.*, **45** [8] 1377–80 (1991).
[38]R. K. Sato, J. Bolvin, and P. F. McMillan, "Synthesis and Characterization of a SiAlON Glass," *J. Am. Ceram. Soc.*, **73** [8] 2494–97 (1990).
[39]M. L. Hair, *Infrared Spectroscopy in Surface Chemistry*; pp. 79–139. Marcel Dekker, New York, 1967.
[40]D. L. Wood and E. M. Rabinovich, "Study of Alkoxide Silica Gels by Infrared Spectroscopy," *Appl. Spectrosc.*, **43** [2] 263–67 (1989).
[41]V. S. Nguyen, S. Burton, and P. Pan, "The Variation of Physical Properties of Plasma-Deposited Silicon Nitride and Oxynitride with Their Compositions," *J. Electrochem. Soc.*, **131** [10] 2348–53 (1984).
[42]G. A. Ruggles, R. Koba, and R. E. Tressler, "Properties of SiO_2 on Si after Exposure to 3:1 H_2 + N_2 and NH_3," *J. Electrochem. Soc.*, **133** [12] 2549–54 (1986).
[43]J. P. Luongo, "IR Study of Amorphous Silicon Nitride Films," *Appl. Spectrosc.*, **38** [2] 195–99 (1984).
[44]R. K. Brow and C. G. Pantano, "Compositionally Dependent Si 2*p* Binding Energy Shifts in Silicon Oxynitride Thin Films," *J. Am. Ceram. Soc.*, **69** [4] 314–16 (1986).
[45](a) R. K. Brow and C. G. Pantano, "Thermochemical Nitridation of Microporous Silica Films in Ammonia," *J. Am. Ceram. Soc.*, **70** [1] 9–14 (1987). (b) H. Du, R. E. Tressler, and K. E. Spear, "Thermodynamics of the Si-N-O System and Kinetic Modeling of Oxidation of Si_3N_4," *J. Electrochem. Soc.*, **136** [11] 3210–15 (1989).
[46]W. Braue, H. J. Dudek, and G. Ziegler, "XPS Study of Glassy Grain Boundary Layers in Dense, High-Strength Silicon Nitride," *J. Non-Cryst. Solids*, **56**, 185–90 (1983).
[47]R. van Weeren, E. A. Leone, S. Curran, L. C. Klein, and S. C. Danforth, "Synthesis and Characterization of Amorphous Si_2N_2O," *J. Am. Ceram. Soc.*, **77** [10] 2699–702 (1994).
[48](a) R. M. Laine, K. Y. Blohowiak, T. R. Robinson, M. L. Hoppe, P. Nardi, J. Kampf, and J. Uhm, "Synthesis of Novel, Pentacoordinate Silicon Complexes from SiO_2," *Lett. Nature*, **353**, 642–44 (1991). (b) K. Y. Blohowiak, M. L. Hoppe, K. W. Chew, P. Kansal, B. L. Mueller, C. L. S. Scotto, T. Hinklin, F. Babonneau, J. Kampf, and R. M. Laine, "SiO_2 as a Starting Material for the Synthesis of Pentacoordinate Silicon Complexes. I," *Chem. Mater.*, **6**, 2177–92 (1994).
[49]Z. F. Zhang, M. L. Hoppe, J. A. Rahn, S. M. Koo, and R. M. Laine, "Low Temperature Routes to Cordierite-like Ceramics using Chemical Processing," *Mater. Res. Soc. Symp. Proc.*, **249**, 107–14 (1992).
[50]C. R. Bickmore, M. L. Hoppe, R. M. Laine, K. A. Y. Blohowiak, P. Nardi, T. R. Robinson, and J. Uhm, "Chemicals, Polymers, and Ceramics from the Beach (Silica)"; pp. 663–70 in *Chemical Processing of Advanced Materials, 5th Conference on Ultrastructure Processing*. Edited by L. L. Hench, J. K. West, and D. R. Ulrich. Wiley, New York, 1992.
[51]G. W. Scherer, "Sintering of Low-Density Glasses: I, Theory," *J. Am. Ceram. Soc.*, **60**, 236–39 (1977).
[52]C. J. Brinker and G. W. Scherer, *Sol–Gel Science: The Physics and Chemistry of Sol–Gel Processing*; Ch. 11. Academic Press, San Diego, CA, 1990.
[53]F. H. P. M. Habraken, A. E. T. Kuiper, Y. Tamminga, and J. B. Theeten, "Thermal Nitridation of Silicon Dioxide Films," *J. Appl. Phys.*, **53**, 6996–7002 (1982). □